Rotationally Supported Virgo Cluster Dwarf Elliptical Galaxies: Stripped Dwarf Irregular Galaxies?

Liese van Zee

Astronomy Department, Indiana University, 727 E 3rd St, Bloomington, IN 47405

vanzee@astro.indiana.edu

Evan D. Skillman

Astronomy Department, University of Minnesota, 116 Church St. SE, Minneapolis, MN 55455

skillman@astro.umn.edu

and

Martha P. Haynes

Center for Radiophysics and Space Research and National Astronomy and Ionosphere Center,¹
Cornell University, Ithaca, NY 14853

haynes@astro.cornell.edu

ABSTRACT

New observations of 16 dwarf elliptical galaxies in the Virgo Cluster indicate that at least seven dEs have significant velocity gradients along their optical major axis, with typical rotation amplitudes of 20-30 km s⁻¹. Of the remaining nine galaxies in this sample, 6 have velocity gradients less than 20 km s⁻¹kpc⁻¹ while the other 3 observations had too low of a signal–to–noise ratio to determine an accurate velocity gradient. Typical velocity dispersions for these galaxies are \sim 44 ± 5 km s⁻¹, indicating that rotation can be a significant component of the stellar dynamics of Virgo dEs. When corrected for the limited spatial extent of the spectral data, the rotation amplitudes of the rotating dEs are comparable to those of similar brightness dIs. Evidence for a relationship between the rotation amplitude and galaxy luminosity is found, and, in fact, agrees well with the Tully-Fisher relation. The similarity in the scaling relations of dIs and dEs implies that it is unlikely that dEs evolve from significantly more luminous galaxies. These observations reaffirm the possibility that some cluster dwarf elliptical galaxies may be formed when the neutral gaseous medium is stripped from dwarf irregular galaxies in

¹The National Astronomy and Ionosphere Center is operated by Cornell University under a cooperative agreement with the National Science Foundation.

the cluster environment. We hypothesize that several different mechanisms are involved in the creation of the overall population of dE galaxies, and that stripping of infalling dIs may be the dominant process in the creation of dEs in clusters like Virgo.

Subject headings: galaxies: clusters: general — galaxies: dwarf — galaxies: evolution — galaxies: kinematics and dynamics

1. Introduction

Dwarf elliptical¹ galaxies (dE) are the most ubiquitous type of galaxy in the local universe (Binggeli et al. 1988; Ferguson & Binggeli 1994; Gallagher & Wyse 1994). Despite their plenitude, we still do not understand fully the formation mechanism of these low mass, gas-poor systems. One clue to the evolution of dwarf elliptical galaxies is the morphology-density relation: similar to giant elliptical galaxies, dwarf elliptical galaxies are found primarily in high density regions such as galaxy clusters, compact groups, and loose groups (Binggeli et al. 1988). However, unlike their giant cousins, the stellar distribution in dwarf elliptical galaxies is exponential in nature (Lin & Faber 1983; Kormendy 1985), indicating that dwarf elliptical galaxies are not just lower mass versions of giant elliptical galaxies. Thus, the evolutionary scenarios proposed for giant elliptical galaxies may not be relevant for the dwarf elliptical class.

While some aspects of galaxy evolution undoubtedly arise from initial conditions, on-going evolution is likely accelerated and affected by different mechanisms in dense cluster environments. As the nearest such location, the Virgo cluster serves as the best laboratory for exploring the details of evolution under intracluster conditions, providing access to spatial scales and mass and luminosity ranges that are not achievable in more distant systems. As discussed in Binggeli et al. (1988), the galaxy population in Virgo is dominated by dwarf galaxies which, because of its proximity, can be identified in large numbers. Thus, Virgo provides an ideal setting for the study of dwarf galaxy evolution in the cluster environment.

A multitude of evolutionary scenarios have been proposed to explain the relationship between gas—poor dwarf elliptical galaxies and gas—rich dwarf irregular galaxies (e.g., Dekel & Silk 1986; Silk et al. 1987; Davies & Phillipps 1988). The key component of these models is the gas removal process: gas is removed either through a "blow—out" following a starburst episode, or via ram pressure stripping as the galaxy encounters the hot intergalactic medium (IGM) or intracluster medium (ICM). Note that the latter method provides a natural explanation to the density-morphology relationship observed in the dwarf galaxies of the Local Group (van den Bergh 1994) and in clusters (Binggeli, Tarenghi, & Sandage 1990), while the former method has difficulty explaining this phenomenon.

¹The term "dwarf elliptical" is used in this paper to indicate the most common type of low mass, gas–poor dwarf galaxy; some authors prefer to use "spheroidal" and "dwarf spheroidal" to describe this class.

Interestingly, if either of the above scenarios are correct, the stellar remnant (dE) should have the same kinematic properties as the progenitor (dI). However, the ground–breaking kinematic work by Bender & Nieto (1990) on dE's in Virgo and Bender et al. (1991) on three dE companions of M31 suggested that this may not be the case for dEs: of the 5 dwarf elliptical galaxies in these two early studies, none are supported by rotation ($V_{rot} < 20 \text{ km s}^{-1}$); in contrast, most dwarf irregular galaxies of comparable mass (or luminosity) are rotationally supported. Recently, however, Mayer et al. (2001a,b) have shown that "tidal stirring" – or repeated tidal shocks suffered by dwarf satellite galaxies – can convert a dI into a dE by both removing its gas and changing it into a dynamically hot galaxy. Thus, lack of rotation in dE galaxies does not exclude the conversion of dI to dE, but may indicate a more catastrophic evolutionary pathway than blow–out or ram pressure stripping alone.

The number of dwarf elliptical galaxies with spatially resolved rotation curves is still quite small, however. Stellar kinematics of large samples of dwarf elliptical galaxies are needed to investigate fully kinematic constraints on evolutionary scenarios. Several projects with modest sample sizes have recently appeared in the literature (e.g., Pedraz et al. 2002; Geha et al. 2002, 2003). Here, we present the first results from a program to measure the stellar kinematics of dwarf galaxies; rotation curves and velocity dispersions of sixteen dwarf elliptical galaxies in the Virgo Cluster are discussed in this paper.

The paper is organized as follows. The spatially resolved kinematic observations are described in Section 2. In Section 3, the observed kinematic properties are compared to those of giant elliptical galaxies and dwarf irregular galaxies. In contrast to previous studies of dEs, seven of the sixteen galaxies in this sample have clear evidence of rotational support. These results are discussed in the context of dwarf galaxy evolution in Section 4. The conclusions of the paper are summarized in Section 5.

2. Kinematic Observations

2.1. Sample Selection

We selected a moderate sized sample of nearby dwarf elliptical galaxies for spatially resolved kinematic observations from the Virgo Cluster Catalog (VCC, Binggeli et al. 1985). The target galaxies were selected based on their apparent magnitude ($m_B < 15.5$), morphological classification (dE), and on their apparent ellipticity ($\epsilon > 0.25$). The latter criterion was imposed to mitigate the affects of disk projection in the measurement of rotational velocities, and it should be noted that its adoption biases the sample toward objects with higher apparent rotation velocity. The implication of this bias in terms of the galaxy evolution scenarios described in Section 4 is uncertain. The sample was further restricted to the luminous dwarf elliptical galaxies in the VCC with measured recessional velocities that place them within the Virgo Cluster (e.g., Conselice et al. 2001), at a distance of approximately 16.1 Mpc (e.g., Kelson et al. 2000). Dynamically young, Virgo is known

to contain several substructural units (Binggeli et al. 1987) and appears to be elongated along the line-of-sight (Yasuda et al. 1997; Solanes et al. 2002). Recent observations of surface brightness fluctuations (Jerjen et al. 2004) have shown that the dE population is stretched in depth similarly to the bright elliptical population (Neilsen & Tsvetanov 2000; West & Blakeslee 2000) but not as extended as claimed previously by Young & Currie (1995). Figure 1 shows the location of the selected galaxies within the Virgo Cluster; the targeted galaxies were selected to include a range of environments within the cluster, sampling both the cluster core and the outer field.

The observational properties of the selected galaxies are tabulated in Table 1. Included in Table 1 are the morphological class from the VCC (Binggeli et al. 1985) and group assignments from Binggeli et al. (1993). The tabulated position angle, ellipticity, apparent magnitude, central surface brightness, and scale length are derived from ELLIPSE fitting of UBVRI images obtained with the VATT 1.8m telescope (van Zee & Barton in prep). We note that the newly derived ellipticities are in excellent agreement with those values previously published for VCC 543, VCC 990, VCC 1122, VCC 1308, VCC 1514, VCC 1743, and VCC 2019 (Ryden et al. 1999).

2.2. Palomar Observations

High resolution optical spectra of the target galaxies were obtained with the Double Spectrograph on the 5m Palomar² telescope on the nights of 2001 March 19-21 and 2002 Apr 8-10. The 6800 Å dichroic was used to split the light to the two sides (blue and red) of the spectrograph. Both sides of the spectrograph were equipped with 1200 l/mm gratings (blazed at 5000 Å on the blue side and blazed at 9400 Å on the red side). The thinned TEK 1024 \times 1024 CCD on the blue side of the spectrograph had a read noise of 8.6 e⁻, a system gain of 2.13, and an angular scale of 0.624 arcsec/pix. The thinned TEK 1024 \times 1024 CCD on the red side of the spectrograph had a read noise of 7.5 e⁻, a system gain of 2.0, and an angular scale of 0.482 arcsec/pix. The blue side was centered at the Mg Ib triplet, with wavelength coverage of 4800 – 5700 Å and an effective resolution of 2.3 Å (0.88 Å/pix). The red side was centered at the Ca triplet, with wavelength coverage of 8250 – 8900 Å and an effective resolution of 1.6 Å (0.64 Å/pix).

A summary of the observations is tabulated in Table 2. The 2' long slit was oriented along the optical major axis of each galaxy. Since the galaxies in this sample are faint and low surface brightness, the telescope was centered on a nearby bright star and then offset to the galaxy position. The slit viewing camera provided confirmation that the slit was aligned and centered appropriately. To improve the sensitivity, the slit was set to a width of 2'' for all observations; the seeing was approximately 1'' during all 6 nights. Due to the low surface brightness nature of the dE galaxies, long integration times (on the order of 2-3 hours per pointing) were necessary to have sufficient

²Observations at the Palomar Observatory were made as part of a continuing cooperative agreement between Cornell University and the California Institute of Technology.

signal-to-noise in the absorption lines to trace the stellar kinematics to large radii.

Observations of standard stars were obtained at the beginning and end of the night. Flux calibration was derived from observations of Feige 34, BD +75 325, and BD +33 2642 (Oke 1990). The nights were non-photometric, but generally transparent. At least 6 radial velocity standards (F7 - K2 giants) were also observed each night in order to create stellar templates for cross-correlation analysis. The radial velocity standards are tabulated in Table 3. During the 2002 April observing run, several stars with low metallicities were targeted in order to verify that spectral differences between the template stars (typically solar metallicity) and the low metallicity dwarf elliptical galaxies did not introduce systematic errors. As expected, we did not find that the metallicity of the template star had a significant effect on the derived redshift or velocity dispersion for these modest dispersion observations.

2.3. Data Reduction

The spectra were reduced and analyzed with the IRAF³ package. The spectral reduction included bias subtraction, scattered light corrections, and flat fielding with both twilight and dome flats. The 2–dimensional (2-d) images were rectified based on arc lamp observations (blue) or night sky lines (red) and the trace of stars at different positions along the slit. Confirmation of the wavelength solution was provided by comparing the observed heliocentric velocities of the radial velocity standards with those found in the literature. A small systematic offset (2 km s⁻¹, or 0.1 pixel) was found between the blue and red spectra and the literature values, which is well within the expected error for these relatively high signal-to-noise stellar observations. The accuracy of the spatial rectification was confirmed by measuring the location of the each galaxy's center of light at several different wavelengths; spatial offsets from one end of the spectra to the other were minimal for both sides of the spectrograph.

Each galaxy observation consisted of multiple 1200 sec exposures. Night sky lines were removed from the two dimensional images before the individual images were averaged together. The final combined images were flux calibrated based on the sensitivity function derived from the flux standards observed each night. One-dimensional (1-d) spectra of the stars and galaxies were extracted from the 2-d spectra using the task APALL. Integrated spectra for each galaxy are shown in Figure 2.

Several different techniques were used to extract kinematic data from the observed spectra. The first technique employed was a straight–forward Gaussian fit to the strongest lines (the 3 Mg Ib lines on the blue side and the Ca triplet on the red side). To improve the signal–to–noise ratio, the 2-d images were boxcar smoothed to a spatial resolution of 1.87"/pix for the blue camera (binned by 3 pixels) and 2.41"/pix for the red camera (binned by 5 pixels). The rotation curves were determined

³IRAF is distributed by the National Optical Astronomy Observatories.

from the centroid of the Gaussian fits and velocity dispersions were determined by subtracting the instrumental width (derived from the standard star observations) in quadrature from the observed line widths. While the values obtained from this simplistic measurement technique are not reported here, the Gaussian fitting procedure provided a baseline value for the rotation curves and velocity dispersion measurements described below.

Fourier analysis provides a more robust measure of the stellar kinematics, particularly when line shapes are not expected to be perfect Gaussian profiles. The rotation curves for each galaxy were derived from cross-correlation analysis of the observed spectra with radial velocity template stars (Table 3). In order to determine which of the radial velocity standards provided the best template match to the galaxy spectra, all of the radial velocity standards observed during the same observing run were cross-correlated with the 1-d galaxy spectra (Figure 2) using the task FXCOR in the RV package. The radial velocity standards were then rank ordered based on the derived Tonry-Davis Ratio (TDR, Tonry & Davis 1979) for each galaxy. The later spectral types (G5 III - K2 III) proved to have the best correlation coefficients when cross correlated with the dwarf elliptical galaxy spectra; in fact, the best template match for both observing runs was HD 65934, a star classified as a G8 III. For both observing runs, the seven stars with the highest average TDR were used in the subsequent analysis.

Prior to further cross–correlation analysis, the 2-d images were boxcar smoothed to a spatial resolution of approximately 2"/pix (see above), 4"/pix, and 8"/pix to increase the signal–to–noise ratio. Each row of each 2-d image was cross–correlated with the selected subset of radial velocity standards using XCOR in the contributed REDSHIFT package of STSDAS. The task XCOR was selected for the final analysis because it returned both a redshift and a velocity dispersion measurement. In this analysis, the derived centroid values were not sensitive to the spectral type of the template star; typical individual differences between the systemic velocity measured by each of the templates were on the order of 6 km s⁻¹ on the red side and 12 km s⁻¹ on the blue side and relative velocity differences were much smaller than that. The systemic heliocentric velocities for each galaxy are tabulated in Table 4. The error estimates quoted in Table 4 are derived from the dispersion of results from the different analysis techniques and cross correlation of the galaxy spectra with different template stars. These errors should be considered indicative of both systematic and random errors; typically, the quoted errors are larger than the formal errors returned by the IRAF tasks.

In general, when smoothed to a spatial resolution of 2"/pix, the galaxy rotation curves could be traced to radii of approximately 20" or 1.56 kpc at the distance of Virgo. There were no significant differences between the rotation curves derived from the Mg Ib and those derived from the Ca triplet lines. The derived rotation curves are shown in Figure 3, with the maximum velocity width denoted by dashed lines. Except for VCC 1075 and VCC 1857, all of the plots in Figure 3 are from the data binned to 2" resolution. Seven of the sixteen galaxies have clear evidence of a velocity gradient across the stellar component; the rotational component is easily discernible in the raw image for all of these galaxies. The slope of the rotation curve was derived from linear regression

analysis of all of the data points (both blue and red cameras) and is tabulated in Table 4. The representative maximum rotation velocity (V_{rot}) was derived from the fitted rotation curve and the maximum radius at which the rotation curve could be measured. The rotation velocities are tabulated in Table 4. Five of the galaxies in the present sample are also included in Geha et al. (2003); in all cases, the present rotation curves trace the galaxy kinematics to a significantly larger radius due to both the limited slit length of the Keck observations and to signal—to—noise ratio concerns. Thus, the derived maximum rotation velocities are larger than previously reported.

The same cross-correlation analysis yielded a velocity dispersion measurement for each galaxy. The velocity dispersion measurements were calibrated by analyzing the artificially broadened spectra of one of the template stars. Based on the stellar template, observations with the blue camera did not have sufficient resolution to provide accurate velocity dispersion measurements of these galaxies, while the Ca line observations had sufficient resolution to measure velocity dispersions greater than 35 km s⁻¹. The measured velocity dispersions are shown in Figure 3 and the central (σ_0) and median (σ_m) values are tabulated in Table 4. The median velocity dispersion is derived from the average of the measurements at all radii. The typical velocity dispersion for the galaxies in this sample is 44 ± 5 km s⁻¹. In general, given the relatively poor spectral resolution of both cameras and low velocity dispersions of the galaxies, the reported velocity dispersions should be considered indicative upper limits.

For comparison, three of these galaxies have velocity dispersions in the published literature [VCC 543 and VCC 1122, Bender et al. (1992) and Pedraz et al. (2002); VCC 917, Geha et al. (2002)]. The mean velocity dispersion for VCC 1122 reported in Bender et al. (1992) is larger than the value reported here, but is consistent with the central velocity dispersion measurement. Figure 4 shows a direct comparison of the line shape expected for a template star broadened by the velocity dispersion for the integrated spectrum of VCC 1122; the derived velocity dispersion is clearly a good match to the observed spectra. The velocity dispersion of VCC 543 reported here is comparable to that of Bender et al. (1992); similar good agreement is found between the new observations of VCC 917 and those reported in Geha et al. (2002), although the reported systemic velocity of VCC 917 is significantly different than that reported here.

3. Rotation in Dwarf Elliptical Galaxies

The derived rotation velocities and velocity dispersions indicate that several dwarf elliptical galaxies in the Virgo cluster have significant rotation components. The ratio of the rotation velocity to velocity dispersion for the Virgo dwarf elliptical galaxies is shown in Figure 5 and tabulated in Table 4. Note, however, that the anisotropy parameters, $(v/\sigma_m)^*$, listed in Table 4 and shown in Figure 5 should be considered representative lower limits for the dEs. Not only are the derived velocity dispersions representative upper limits, the present observations only sampled the kinematics along the major axis; if the dEs have a significant velocity gradient along a different axis, such as found in some dI galaxies [e.g., NGC 625, (Côté, Carignan, & Freeman 2000) and NGC 5253,

(Kobulnicky & Skillman 1995)], the derived anisotropy parameters will be underestimates of their true values. Also shown in Figure 5 are the anisotropy parameters for giant elliptical galaxies from Bender et al. (1992) and the dwarf elliptical galaxies in Pedraz et al. (2002), Geha et al. (2002), Simien & Prugniel (2002), and De Rijcke et al. (2001, 2003). Five of the dwarf elliptical galaxies in the Virgo sample have a significant rotation component. These galaxies overlap the locus of anisotropy parameters found in giant elliptical galaxies, where the lower luminosity ellipticals tend to have large anisotropy parameters. Eight of the remaining dwarf elliptical galaxies have modest anisotropy parameters, while only one, VCC 1261, has an extremely low value. These results are significantly different than those reported by Geha et al. (2002) and the early studies of Bender & Nieto (1990) and Bender et al. (1991) where it appeared that dwarf elliptical galaxies had no significant rotation component. However, the recent observations by Pedraz et al. (2002) and Geha et al. (2003) revealed a handful of dwarf elliptical galaxies with significant rotation. Thus, it appears that the kinematics of some dwarf elliptical galaxies are dominated by rotation, not random motions.

While this result is counter to the results reported in earlier studies, it should not be surprising. The dwarf elliptical galaxies in this sample are all located in the region of strong overdensity that characterizes the Virgo Cluster. It is well known that galaxies located near the cluster center are deficient in neutral hydrogen relative to their counterparts in the field (e.g., Giovanelli & Haynes 1983; Solanes et al. 2001). For giant spiral galaxies, the loss of their ISM may result in modest morphological changes, including suppression of their star formation activity (e.g., Koopmann & Kenney 1998). However, despite these changes, gas-deficient giant spiral galaxies are likely still to be classified as spiral galaxies since there are striking morphological differences between giant spiral and elliptical galaxies. This is not the case for dwarf galaxies. Dwarf elliptical galaxies and dwarf irregular galaxies share common morphological parameters; both have approximately exponential surface brightness profiles and have similar central surface brightnesses and scale lengths (see Section 4 for further discussion of the similarities between dEs and dIs). Thus, their structural parameters do not provide a strong morphological distinction between dwarf elliptical galaxies and dwarf irregular galaxies; rather, their morphological classification is highly dependent on the patchy appearance (or absence thereof) due to irregular star formation activity across the surface of the galaxy. If star formation ceases in a dwarf galaxy, the resulting system is likely to be classified as a dwarf elliptical galaxy once the massive stars, which provide the patchy contrast, have evolved off of the main sequence. In fact, it is this morphological commonality that first led to the idea that dwarf elliptical galaxies could evolve passively from dwarf irregular galaxies after a starburst episode (e.g., Lin & Faber 1983; Kormendy 1985; Loose & Thuan 1986; Drinkwater & Hardy 1991; James 1994; Papaderos et al. 1996a; Sung et al. 1998).

If the dwarf elliptical galaxies in this sample are the end products of dwarf irregular galaxies which have been stripped of their ISM, the observed rotation velocities should be similar to the rotation velocities of normal dwarf irregular galaxies. The correlation between rotation width (corrected for inclination) and absolute magnitude for the dwarf elliptical galaxies is shown in Figure

6. Also shown in Figure 6 are the values for dwarf irregular galaxies compiled in van Zee (2001) and the correlation derived for spiral galaxies (Tully & Pierce 2000). In general, dwarf irregular galaxies have a large scatter in the Tully-Fisher diagram, in part due to uncertain inclination and velocity dispersion corrections. However, there is still a general trend that more luminous dwarf irregular galaxies have larger rotation widths. Many of the dwarf elliptical galaxies also appear to follow this trend; the exceptions are VCC 917, 1122, 1261, 1308, 1514, and 2050, which are underrotating for their observed luminosity. These galaxies all have kinematic slopes which are less than 20 km s⁻¹ kpc⁻¹; we designate these galaxies as the "non-rotating" sample. Those that follow the Tully-Fisher relation (VCC 178, 437, 543, 965, 990, 1036, 2019) are designated the "rotationally supported" sample. Note that VCC 1743 and VCC 1857 also appear to be rotationally supported, but their observations are too poor quality to include in the statistics. These groupings are similar to those seen in the anisotropy diagram (Figure 5), with the exception that VCC 178 and 965 fall in the "modest" $(v/\sigma_m)^*$ grouping. We elect to separate the kinematic samples based on the amplitude of the slope of the rotation curve and location in the Tully-Fisher diagram since the velocity dispersion measurements are not as secure as the rotation curve measurements for these observations.

Note that Figure 6 compares stellar (dE) and gaseous (dI and spirals) rotation curves. While the stars and gas are expected to be kinematically coupled in normal galaxies, it is necessary to consider whether the stellar rotation curves sample fully the rotation velocities of these galaxies. As mentioned above, the observations were limited to the optical major axis; for most galaxies, this is the axis with the largest velocity gradient, and thus it is reasonable to assume that the rotation curves measured here are representative. However, the stellar rotation curves were traced out to only a modest radius whereas the neutral gas velocity widths include emission from gas that extends well beyond the optical galaxy. Nonetheless, if the dwarf elliptical galaxies and dwarf irregular galaxies have similar kinematic properties, it should be possible to correct for this effect on a statistical basis.

For comparison, we consider the neutral gas distribution and kinematics for a sample of 20 galaxies selected from the optical imaging samples of van Zee et al. (1997a) and van Zee (2001), i.e., a subset of the dwarf irregular galaxies shown in Figure 6. The resolved HI distribution and kinematics were obtained with Very Large Array during several observing runs from 1993 - 2000. While the majority of the HI synthesis data is as yet unpublished, the dI sample includes the galaxies in van Zee et al. (1997b) with distances scaled to an H_0 of 75 km s⁻¹ Mpc⁻¹. A histogram of the extent of the HI distribution to optical scale length for the dI sample is shown in Figure 7a. To determine the statistical correction to convert from a stellar rotation width to a neutral gas rotation width, we measured the ratio of the maximum rotation velocity to the slope of the rotation curve. A histogram of the V_{max} /slope for dwarf irregular galaxies is shown in Figure 7b, where the slope of the rotation curve is in units of km s⁻¹ per scale length. The mean value is 2.45 ± 0.58 scale lengths, which shows remarkable (and perhaps co-incidental) agreement with the use of the velocity at 2.2 scale lengths as a fiducial measure of spiral galaxy rotation curves (e.g.,

Courteau & Rix 1999). Based on these results, it is likely that the stellar rotation curves obtained here underestimate the maximum rotation velocity for the dwarf elliptical galaxies since most were traced out to only 1 - 1.5 scale lengths. Arrows in Figure 6 indicate the location of each galaxy if the stellar rotation curves were traced to 2.45 scale lengths and the galaxy dynamics follow similar trends as those of the neutral gas in dI galaxies.

Given the uncertainties associated with this velocity width correction, it is premature to draw far reaching conclusions from the revised velocity widths. Nonetheless, it is important to note that such measurements could provide significant constraints on the luminosity evolution of dE galaxies. In particular, these rough correction factors indicate that the progenitor galaxies were at most only 2 magnitudes more luminous than the present population (i.e., the revised rotation widths are comparable to those of galaxies 2 magnitudes more luminous). If these results are confirmed by observations that fully trace the galaxy dynamics, the progenitor population of Virgo dEs must be restricted to moderate luminosity systems. In particular, it is unlikely that dEs evolve from significantly more luminous galaxies.

4. Dwarf Galaxy Evolution Scenarios

One of the perplexing issues in galaxy evolution is the remarkable commonality between dwarf elliptical galaxies and dwarf irregular galaxies. These low mass systems have similar stellar distributions, both in terms of functional form (exponential) and in terms of typical central surface brightnesses and scale lengths (Lin & Faber 1983). Furthermore, both dIs and dEs follow the same luminosity-metallicity relation, where the more luminous galaxies are more metal rich, regardless of their gas content (Skillman, Kennicutt, & Hodge 1989; Richer & McCall 1995). In fact, aside from their current gas content and star formation activity, the low mass galaxy classes are remarkably similar in stellar content and morphology.

As mentioned in the introduction, the apparent morphological similarity between the low mass galaxy classes led to several possible evolutionary scenarios that linked dwarf irregular galaxies and dwarf elliptical galaxies. However, the apparent kinematic mis-match between dEs and dIs posed a severe constraint for evolutionary pathways between dIs and dEs since angular momentum must be conserved (see, e.g., Bender et al. 1991; Skillman & Bender 1995; van Zee et al. 2001). However, the early studies included only a small number of dEs. The new observations presented here indicate a remarkable similarity between the kinematic properties of many dwarf elliptical and dwarf irregular galaxies; these results re-open the possibility that some dEs are formed from passive evolution of dIs⁴.

To some degree, the question of whether dwarf elliptical galaxies evolve from dwarf irregular

⁴In this context, passive evolution is taken to mean simple evolution of the stellar population without a major merger or other catastrophic event.

galaxies is tautological since every dE must have been gas-rich and star-forming at some point in the past. Standard morphological classification would identify these gas-rich, low mass galaxies as dIs. Thus, the relevant question is not whether a dE evolves from a dI, but what caused the progenitors of dEs to stop forming stars and to lose their ISM.

One popular scenario is that the progenitors were too low mass to retain their ISM after a star formation episode (e.g. Dekel & Silk 1986; De Young & Gallagher 1990). In this scenario, the kinetic energy from supernovae explosions is sufficient to sweep out the remaining ISM after a starburst episode. However, more recent calculations indicate that it may be more difficult to remove the ISM of a dark matter dominated galaxy than previously thought (e.g., De Young & Heckman 1994; Silich & Tenorio-Tagle 1998; Mac Low & Ferrara 1999; Ferrara & Tolstoy 2000). Furthermore, detailed star formation histories of nearby dwarf Spheroidal galaxies indicate these extremely low mass galaxies were able to retain their ISM through several star formation episodes (e.g., Carina dSph, Smecker-Hane et al. 1994). Thus, internal gas-loss mechanisms face several challenges to explain the diversity of stellar populations, the relative chemical enrichment, and the relative gas-richness of low mass galaxies.

Alternatively, the key to the formation of dwarf elliptical galaxies may be an external process. Dwarf elliptical galaxies are the most strongly clustered galaxy type (Ferguson & Sandage 1989). They are predominantly found in high density regions, either in galaxy clusters or located near more massive spiral and elliptical galaxies. Given the strong morphology-density relation for dwarf elliptical galaxies, it is reasonable to assume that the environment may play a crucial role in their evolution. Segregation within the dwarf ellipticals in Virgo itself has already been noted by several authors (Ferguson & Sandage 1989; Oh & Lin 2000), who point out that the nucleated dE's occupy the cluster core, whereas the majority of non-nucleated ones are found in the peripheral regions. Furthermore, as discussed in Section 3, ram pressure stripping is an efficient mechanism to remove the ISM from cluster members, regardless of total mass. Infall of galaxies into the Virgo Cluster is an ongoing process (Tully & Shaya 1984; Conselice et al. 2003); one thus expects that small groups of galaxies similar to the Local Group continue to fall into the Virgo Cluster. Given the simple surface mass density criteria for ram pressure stripping (Gunn & Gott 1972), essentially all low mass dwarf irregular galaxies falling into the Virgo cluster will be stripped of their gas (e.g., Marcolini, Brighenti, & D'Ercole 2003). Indeed, there is evidence of a very recent case of stripping of a Virgo dwarf galaxy (UGC 7636, Sancisi, Thonnard, & Ekers 1987; Patterson & Thuan 1992). Unless one imagines that all dwarf galaxies that fall into the Virgo cluster are already dEs (and the fact that they are falling in from low density environments argues strongly against this), then it would appear to be inevitable that some of the dEs in the Virgo cluster are stripped dIs.

Since dwarf irregular galaxies are dark matter dominated, removal of their ISM will have only a modest effect on their kinematics. However, subsequent passages through the cluster could further disrupt the stellar kinematics via galaxy harassment or merging events. Thus, if dIs are converted into dEs via ram pressure stripping, one might expect a correlation between the location of dwarf elliptical galaxies with significant rotation and the cluster center. While the present

sample is relatively small, Figure 8 shows a hint of such a relationship, in the sense that galaxies with little-to-no rotation appear to be located predominantly in the cluster core or in high density clumps, while those with significant rotation are in the outskirts of the cluster. This is consistent with the idea that gas-rich dwarf galaxies are stripped of their gas during a passage through the intracluster medium; the non-rotating dwarf elliptical galaxies may be remnants of gas-rich systems that have made multiple passes through the ICM, or had a catastrophic event occur. We caution, however, that the present sample size is relatively small and biased toward the more luminous cluster dEs; further observations of a larger sample of dwarf elliptical galaxies throughout the cluster environment are needed to investigate this suggestive trend.

Although we have argued above that the available observations do not allow us to establish the relative strengths of the rotationally supported and non-rotationally supported dE populations, we cannot close without some speculation on the presence of non-rotating dE galaxies. Following the same line of argument given above, i.e., that it is almost inescapable that some of the dEs observed in the Virgo cluster must have lost their gas to ram pressure stripping, it is also likely that some dwarf galaxies entered the Virgo cluster as dEs before they encountered sufficient hot gas for stripping. It also seems inescapable that some dI galaxies interact tidally with more massive galaxies, and thereby lose gas in this manner. Given that it is difficult to quantify the relative importance of these three different channels of cluster dE galaxy formation, we caution against single channel evolutionary scenarios. Specifically, we note that explanations for the densitymorphology relationship in the Local Group may be irrelevant for the cluster density-morphology relationship. A more comprehensive study of kinematics in dE galaxies in both environments is warranted. Based on the data in hand, however, it is clear that environmental pathways for dI to dE conversion must be considered; if further observations support the trend indicated in Figure 8, relevant theories for the formation and evolution of dwarf galaxies must include environmental factors as well as internal processes.

5. Conclusions

We present long-slit optical spectroscopy along the major axis of 16 dwarf elliptical galaxies in the Virgo Cluster. The major results of these observations are as follows:

- (1) Approximately half of the Virgo dE sample has a significant rotation component, with rotation curve slopes $> 20 \text{ km s}^{-1}\text{kpc}^{-1}$.
- (2) Five of the 14 galaxies with measured velocity dispersions have anisotropy parameters $(v/\sigma_m)^* > 1$., indicating significant rotational flattening. Only one of the remaining 9 dEs has $(v/\sigma_m)^* < 0.3$. The remainder have modest anisotropy parameters, indicating that rotational flattening may be significant for the majority of dwarf elliptical galaxies in this sample.
- (3) Based on the observed maximum rotation velocities, the rotating dwarf galaxies appear to follow the Tully-Fisher relation for gas-rich dwarf and spiral galaxies.

These kinematic results re-open the possibility that dwarf elliptical galaxies may be the end products of dwarf irregular galaxies that have lost their ISM via ram pressure stripping or other non-catastrophic processes. The morphological similarities between gas-rich dwarf irregular galaxies and gas-poor dwarf elliptical galaxies appear to extend beyond the stellar distributions and metal enrichment; many gas-rich and gas-poor dwarf galaxies have common dynamical properties, as would be expected for passive evolution models.

We dedicate this paper in memory of J. Bev Oke, whose spectrographs have enabled a plethora of science for many decades and whose dedication and kindness encouraged several generations of scientists to use those spectrographs well. LvZ thanks Elizabeth Barton for many thought-provoking conversations about galaxy formation and evolution. This research has made use of the NASA/IPAC Extragalactic Database (NED) which is operated by the Jet Propulsion Laboratory, California Institute of Technology, under contract with the National Aeronautics and Space Administration. LvZ acknowledges partial support from the Herzberg Institute of Astrophysics and the National Research Council of Canada; LvZ also acknowledges partial support from Indiana University. EDS is grateful for partial support from a NASA LTSARP grant No. NAG5-9221 and the University of Minnesota. MPH has been supported by NSF grants AST-9900695 and AST-0307396.

REFERENCES

Bender, R., Burstein, D., & Faber, S. M. 1992, ApJ, 399, 462

Bender, R., & Nieto, J.-L. 1990, A&A, 239, 97

Bender, R., Paquet, A., & Nieto, J.-L. 1991, A&A, 246, 349

Binggeli, B., Popescu, C. C., & Tammann, G. A., 1993, A&AS, 98, 275

Binggeli, B., Sandage, A. & Tammann, G. A. 1985, AJ, 90, 1681

Binggeli, B., Sandage, A. & Tammann, G. A. 1988, ARA&A, 26, 509

Binggeli, B., Tammann, G. A. & Sandage, A. & 1987, AJ, 94, 251

Binggeli, B., Tarenghi, M., & Sandage, A. 1990, A&A, 228, 42

Conselice, C. J., O'Neil, K., Gallagher, J. S., & Wyse, R. F. G. 2003, ApJ, 591, 167

Conselice, C. J., Gallagher, J. S., & Wyse, R. F. G. 2001, ApJ, 559, 791

Côté, S., Carignan, C., & Freeman, K. C. 2000, AJ, 120, 3027

Courteau, S. & Rix, H.-W. 1999, ApJ, 513, 561

Davies, J. I., & Phillipps, S. 1988, MNRAS, 233, 553

De Rijcke, S., Dejonghe, H., Zeilinger, W. W., & Hau, G. K. T. 2001, ApJ, 559, L21

De Rijcke, S., Dejonghe, H., Zeilinger, W. W., & Hau, G. K. T. 2003, A&A, 400, 119

De Young, D. S., & Heckman, T. M. 1994, ApJ, 431, 598

De Young, D. S., & Gallagher, J. S. 1990, ApJ, 356

Dekel, A., & Silk, J. 1986, ApJ, 303, 39

Drinkwater, M., & Hardy, E. 1991, AJ, 101, 94

Ferrara, A., & Tolstoy, E. 2000, MNRAS, 313, 291

Ferguson, H. C., & Binggeli, B. 1994, A&A Rev., 6, 67

Ferguson, H. C., & Sandage, A. 1989, ApJ, 346, 53

Gallagher, J. S. & Wyse, R. F. G. 1994, PASP, 106, 1225

Geha, M., Guhathakurta, P., & van der Marel, R. P. 2002, AJ, 124, 3073

Geha, M., Guhathakurta, P., & van der Marel, R. P. 2003, AJ, 126, 1794

Giovanelli, R., & Haynes, M. P. 1983, AJ, 88, 881

Gunn, J. E. & Gott, J. R. I. 1972, ApJ, 176, 1

James, P. A. 1994, MNRAS, 269, 176

Jerjen, H., Binggeli, B. & Barazza, F.D. 2004, AJ, 127, 771

Kelson, D. D. et al. 2000, ApJ, 529, 768

Kobulnicky, H. A., & Skillman, E. D. 1995, ApJ, 454, L121

Koopmann, R. A., & Kenney, J. D. P. 1998, ApJ, 497, L75

Kormendy, J. 1985, ApJ, 295, 73

Lin, D. N. C. & Faber, S. M. 1983, ApJ, 266, L21

Loose, H.-H., & Thuan, T. X. 1986, ApJ, 309, 59

Mac Low, M.-M., & Ferrara, A. 1999, ApJ, 513, 142

Marcolini, A., Brighenti, F., & D'Ercole, A. 2003, MNRAS, 345, 1329

Mayer, L., Governato, F., Colpi, M., Moore, B., Quinn, T., Wadsley, J., Stadel, J., & Lake, G. 2001a, ApJ, 547, L123

Mayer, L., Governato, F., Colpi, M., Moore, B., Quinn, T., Wadsley, J., Stadel, J., & Lake, G. 2001b, ApJ, 559, 754

Neilsen, E.H. Jr. & Tsvetanov, Z.I. 2000, ApJ, 536, 155

Oh, K.S. & Lin, D.N.C 2000, ApJ, 543, 620

Oke, J. B. 1990, AJ, 99, 1621

Papaderos, P., Loose, H.-H., Fricke, K. J., & Thuan, T. X. 1996a, A&A, 314, 59

Patterson, R. J. & Thuan, T. X. 1992, ApJ, 400, L55

Pedraz, S., Gorgas, J., Cardiel, N., Sánchez-Blázquez, P., & Guzmán, R. 2002, MNRAS, 332, L59

Richer, M. G., & McCall, M. L. 1995, ApJ, 445, 642

Ryden, B. S., Terndrup, D. M., Pogge, R. W., & Lauer, T. R. 1999, ApJ, 517, 650

Sancisi, R., Thonnard, N., & Ekers, R. D. 1987, ApJ, 315, L39

Silich, S. A., & Tenorio-Tagle, G. 1998, MNRAS, 299, 249

Silk, J., Wyse, R. F. G., Shields, G. A. 1987, ApJ, 322, L59

Simien, F. & Prugniel, P. 2002, A&A, 384, 371

Skillman, E. D., & Bender, R. 1995, Rev. Mex. AASC, 3, 25

Skillman, E. D., Kennicutt, R. C., & Hodge, P. W. 1989, ApJ, 347, 875

Smecker-Hane, T. A., Stetson, P. B., Hesser, J. E., & Lehnert, M. D. 1994, AJ, 108, 507

Solanes, J.-M., Manrique, A., García-Gómez, C., González-Casado, G., Giovanelli, R., & Haynes, M. P. 2001, ApJ, 548, 97

Solanes, J.-M., Sanchis, T., Salvador-Solé, Giovanelli, R., & Haynes, M. P. 2002, AJ, 124, 2440

Sung, E.-C., Han, C., Ryden, B. S., Chun, M.-S., & Kim, H.-I. 1998, ApJ, 499, 140

Tonry, J., & Davis, M. 1979, AJ, 84, 1511

Tully, R. B., & Pierce, M. J. 2000, ApJ, 533, 744

Tully, R. B. & Shaya, E. J. 1984, ApJ, 281, 31

van den Bergh, S. 1994, ApJ, 428, 617

van Zee, L. 2001 AJ, 121, 2003

van Zee, L., & Barton, E. G. 2004, in prep

van Zee, L., Haynes, M. P., & Salzer, J. J. 1997a, AJ, 114, 2479

van Zee, L., Haynes, M. P., Salzer, J. J., & Broeils, A. H. 1997b, AJ, 113, 1618

van Zee, L., Salzer, J. J., & Skillman, E. D. 2001, AJ, 122, 121

West, M.J. & Blakeslee, J.P. 2000, ApJ, 543, L27

Yasuda, N., Fukugita, M. & Okamura, S. 1997, ApJS, 108, 417

Young, C. K. & Currie, M. J. 1995, MNRAS, 273, 1141

This preprint was prepared with the AAS $\mbox{\sc IAT}_{\mbox{\sc E}}\mbox{\sc X}$ macros v5.2.

Table 1. Properties of the Selected Virgo Dwarf Elliptical Galaxies

Galaxy	Alternative Name	RA (2000)	Dec (2000)	Virgo Assoc.	Morph. Class.	$m_{\mathbf{B}}$	PA	ε	$\begin{array}{c} \mu_B^0 \\ [\mathrm{mag/sq.~"}] \end{array}$	$lpha_B$ ["]
VCC 178	IC 3081	12 16 09.1	12 41 28	Ab	dE5,N	15.81 ± 0.04	86 ± 1	0.42 ± 0.02	21.97	6.7
VCC 437	UGC 7399A	12 20 48.8	17 29 13	Ab	$_{ m dE5,N}$	14.38 ± 0.04	76 ± 3	0.35 ± 0.09	22.86	20.4
VCC 543	UGC7436	$12\ 22\ 19.5$	$14\ 45\ 39$	Ab	dE5	14.58 ± 0.05	120 ± 3	0.44 ± 0.02	22.70	15.8
VCC 917	IC 3344	$12\ 26\ 32.4$	13 34 43	As	dE6	15.68 ± 0.03	58 ± 1	0.44 ± 0.06	22.17	7.8
VCC 965	IC 3363	$12\ 27\ 02.9$	$12\ 33\ 37$	Ab	dE7,N	15.72 ± 0.04	126 ± 2	0.49 ± 0.08	23.16	13.6
VCC 990	IC 3369	$12\ 27\ 16.9$	16 01 30	Ab	dE4,N	14.85 ± 0.05	135 ± 1	0.30 ± 0.04	21.20	6.8
VCC 1036	NGC 4436	$12\ 27\ 41.2$	$12\ 17\ 58$	As	dE6/dS0,N	14.18 ± 0.03	113 ± 1	0.52 ± 0.05	22.38	16.9
VCC 1075	IC 3383	$12\ 28\ 12.3$	$10\ 17\ 53$	Ab	$_{ m dE4,N}$	15.34 ± 0.05	27 ± 1	0.32 ± 0.02	22.34	9.4
VCC 1122	IC 3393	12 28 41.7	$12\ 54\ 57$	Ab	dE7,N	15.09 ± 0.04	132 ± 1	0.53 ± 0.06	22.43	11.5
VCC 1261	NGC 4482	12 30 10.3	$10\ 46\ 47$	As	dE,N	13.78 ± 0.04	134 ± 1	0.37 ± 0.06	21.72	14.9
VCC 1308	IC 3437	$12\ 30\ 45.9$	$11\ 20\ 37$	As	dE,N	15.83 ± 0.04	66 ± 1	0.32 ± 0.06	22.03	7.2
VCC 1514	CGCG 042-152	$12\ 33\ 37.7$	$07\ 52\ 19$	В	dE7,N	15.59 ± 0.04	7 ± 1	0.65 ± 0.03	23.28	13.5
VCC 1743	IC 3602	$12\ 38\ 06.8$	$10\ 04\ 57$	Ab	dE6	15.92 ± 0.04	131 ± 1	0.55 ± 0.02	22.64	8.6
VCC 1857	IC 3647	$12\ 40\ 53.1$	$10\ 28\ 34$	Ab	dE	15.34 ± 0.05	136 ± 5	0.55 ± 0.04	23.27	15.4
VCC 2019	IC 3735	$12\ 45\ 20.4$	$13\ 41\ 35$	Ab	E?	14.78 ± 0.04	152 ± 6	0.27 ± 0.03	21.80	9.3
VCC 2050	IC 3779	$12\ 47\ 20.7$	$12\ 09\ 59$	Ab	dE5:,N	15.62 ± 0.04	126 ± 1	0.48 ± 0.02	22.21	8.0

Note. — Virgo group assignment from Binggeli et al. (1993); morphological classification from Binggeli et al. (1985); m_B , PA, ellipticity, central surface brightness, and scale length were measured from images obtained with the VATT 1.8m (van Zee & Barton, in prep).

Table 2. Observation Log

Galaxy	UT Date	Slit PA	${ m T_{Int}} \ [m sec]$
VCC 178	2001 Mar 20	82	9 × 1200
VCC 437	$2001~\mathrm{Mar}~19$	73	8×1200
VCC 543	$2001~\mathrm{Mar}~21$	119	6×1200
VCC 917	$2001~\mathrm{Mar}~21$	61	6×1200
VCC 965	$2001~\mathrm{Mar}~20$	126	9×1200
VCC 990	$2002~\mathrm{Apr}~8$	133	7×1200
VCC 1036	$2002~\mathrm{Apr}~9$	113	7×1200
VCC 1075	$2002~\mathrm{Apr}~10$	25	1×1200
VCC 1122	$2001~\mathrm{Mar}~19$	134	9×1200
VCC 1261	2002 Apr 10	133	6×1200
VCC 1308	$2002~\mathrm{Apr}~9$	66	10×1200
VCC 1514	$2002~\mathrm{Apr}~8$	7	9×1200
VCC 1743	$2001~\mathrm{Mar}~21$	128	1×1200
VCC 1857	$2001~\mathrm{Mar}~20$	138	1×1200
VCC 2019	$2002~\mathrm{Apr}~10$	158	8×1200
VCC 2050	2001 Mar 21	128	7×1200

Table 3. Radial Velocity Standards

Star Name	Spectral Type	Observing Run	Notes
HD 86801	G0 V	both	
HD 154417	G0 V	2001	
HD 105546	G2 III $[M/H] = -1.6$	2002	
HD 145001	G5 III	both	
HD 144579	G8 V	2001	
$\mathrm{HD}\ 65934$	G8 III	both	best match template star
HD 103545	K0 [M/H] = -2.3	2002	
HD 132737	K0 III	both	
HD 90861	K2 III	both	

Table 4. Kinematic Properties of Virgo Dwarf Elliptical Galaxies

Galaxy	V_{\odot} [km s ⁻¹]	$\begin{array}{c} {\rm Slope} \\ [{\rm km~s^{-1}~kpc^{-1}}] \end{array}$	$V_{\rm rot}$ $[{\rm km~s^{-1}}]$	σ_0 [km s ⁻¹]	$\sigma_{ m m}$ [km s ⁻¹]	(v/σ)*
VCC 178	1120 ± 5	23 ± 3	26 ± 3	46 ± 10	46 ± 5	0.66 ± 0.10
VCC 437	1422 ± 5	25 ± 3	40 ± 5	47 ± 6	50 ± 5	1.11 ± 0.18
VCC 543	984 ± 4	25 ± 2	41 ± 4	38 ± 8	44 ± 5	1.04 ± 0.16
VCC 917	1245 ± 5	10 ± 5	12 ± 6	42 ± 5	40 ± 5	0.35 ± 0.17
VCC 965	826 ± 5	25 ± 4	29 ± 4	42 ± 8	56 ± 15	0.54 ± 0.16
VCC 990	1721 ± 4	26 ± 2	33 ± 3	39 ± 10	43 ± 5	1.17 ± 0.16
$VCC\ 1036$	1132 ± 5	23 ± 1	49 ± 2	34 ± 8	37 ± 4	1.27 ± 0.14
VCC 1075	1818 ± 5			33 ± 9	29 ± 10	
VCC 1122	$470~\pm~6$	18 ± 2	26 ± 3	55 ± 5	40 ± 4	0.61 ± 0.10
VCC 1261	1838 ± 5	1 ± 2	2 ± 3	50 ± 8	48 ± 4	0.05 ± 0.08
VCC 1308	1738 ± 5	12 ± 4	11 ± 3	41 ± 8	40 ± 4	0.39 ± 0.13
VCC 1514	579 ± 5	12 ± 2	21 ± 4	46 ± 7	48 ± 6	0.33 ± 0.08
VCC 1743	$1273~\pm~7$	41 ± 24	33 ± 19	27 ± 11	47 ± 6	0.63 ± 0.38
VCC 1857	695 ± 10	26 ± 7	38 ± 10			
$VCC\ 2019$	1835 ± 6	28 ± 3	31 ± 3	37 ± 7	41 ± 4	1.25 ± 0.17
VCC 2050	1182 ± 7	17 ± 3	18 ± 3	43 ± 5	37 ± 6	0.52 ± 0.12

Note. — V_{\odot} is the heliocentric recessional velocity as measured from cross-correlation analysis of the average galaxy spectrum; the slope of the rotation curve is derived from linear regression analysis of all of the data points (blue and red cameras); $V_{\rm rot}$ is derived from the slope of the rotation curve and the maximum radius at which the rotation curve could be measured, uncorrected for inclination effects, and is also shown graphically in Figure 3; σ_0 is the velocity dispersion of the central 2" of each galaxy; σ_m is the mean velocity dispersion of each galaxy, and is shown graphically in Figure 3; $(v/\sigma)^*$ is the anisotropy parameter and is equal to $(v/\sigma)/\sqrt{\epsilon/(1-\epsilon)}$.

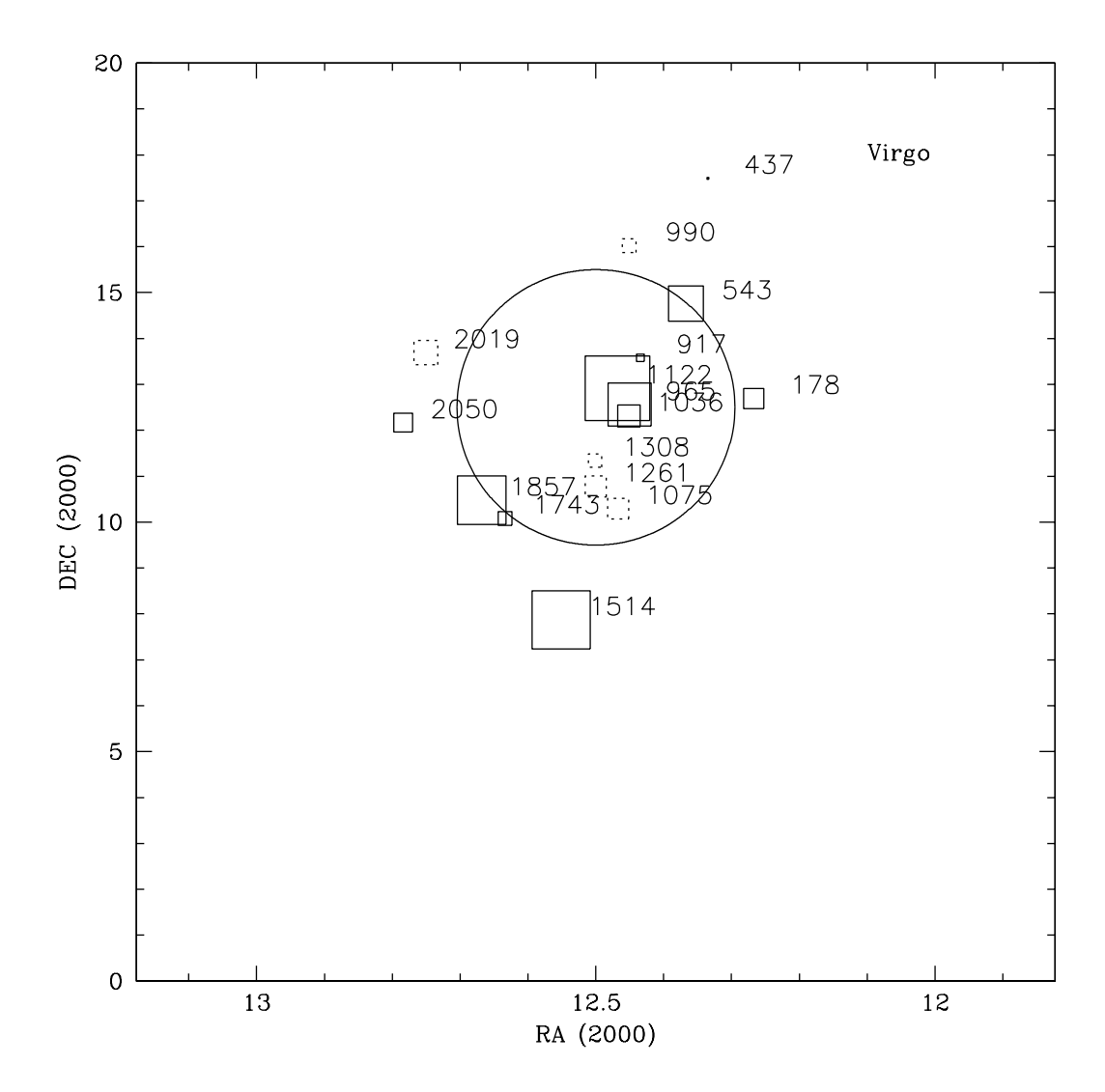


Fig. 1.— Location of the dwarf elliptical galaxies in the Virgo Cluster. The size of the box is indicative of the recessional velocity relative to $1050~\rm km~s^{-1}$, with solid squares indicating galaxies that are blueshifted and dotted squares indicating galaxies that are redshifted relative to this value. The circle denotes the inner 3° radius of the Virgo Cluster. The sample includes dwarf elliptical galaxies in a range of environments within the Virgo Cluster.

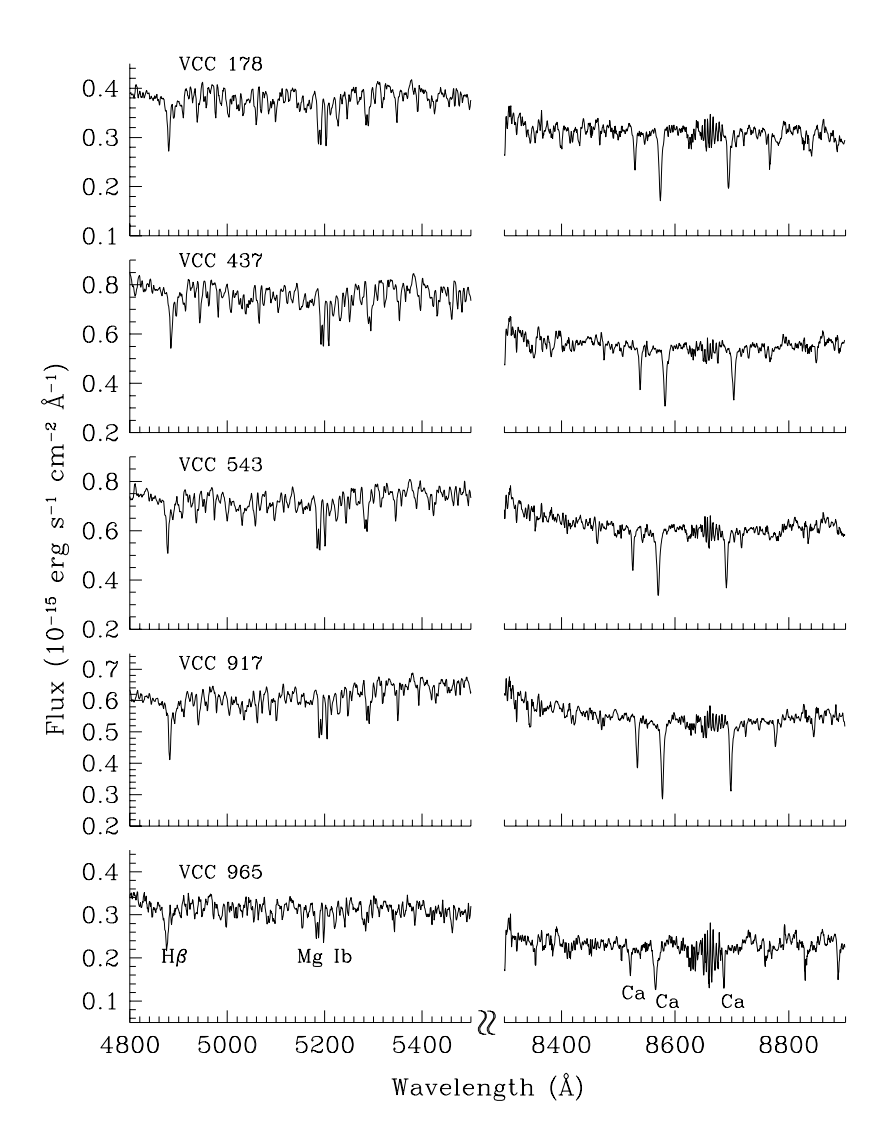
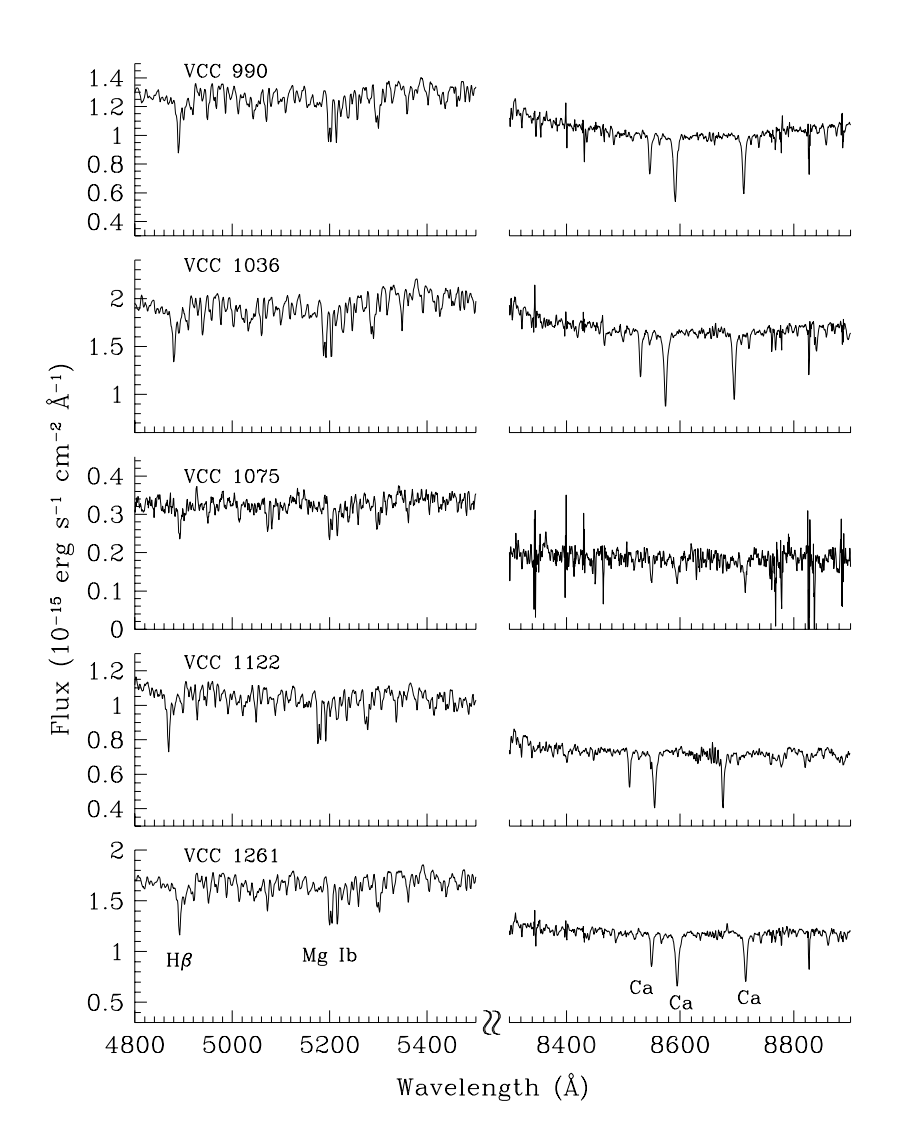
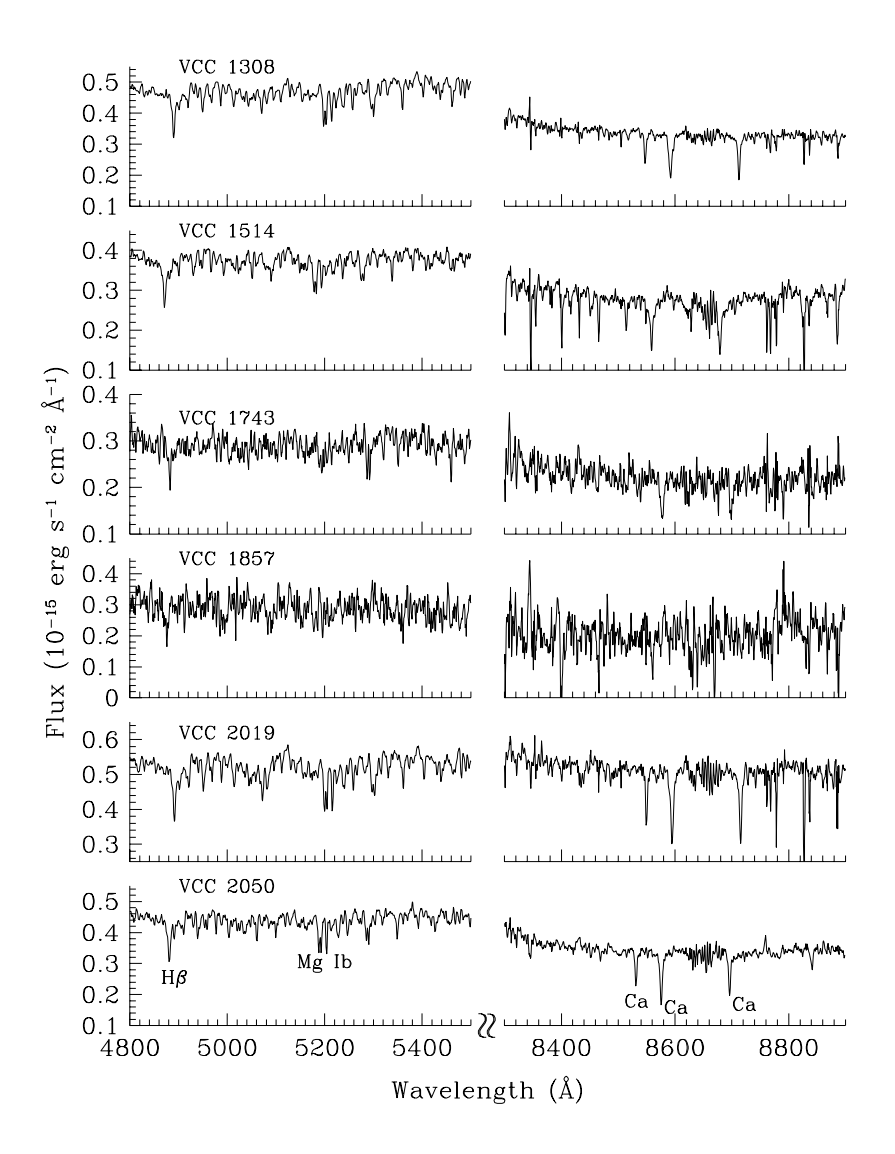


Fig. 2.— Optical spectra of sixteen dwarf elliptical galaxies summed over the entire spatial extent. The Mg Ib and Ca triplet lines were used to trace the stellar kinematics of each galaxy.





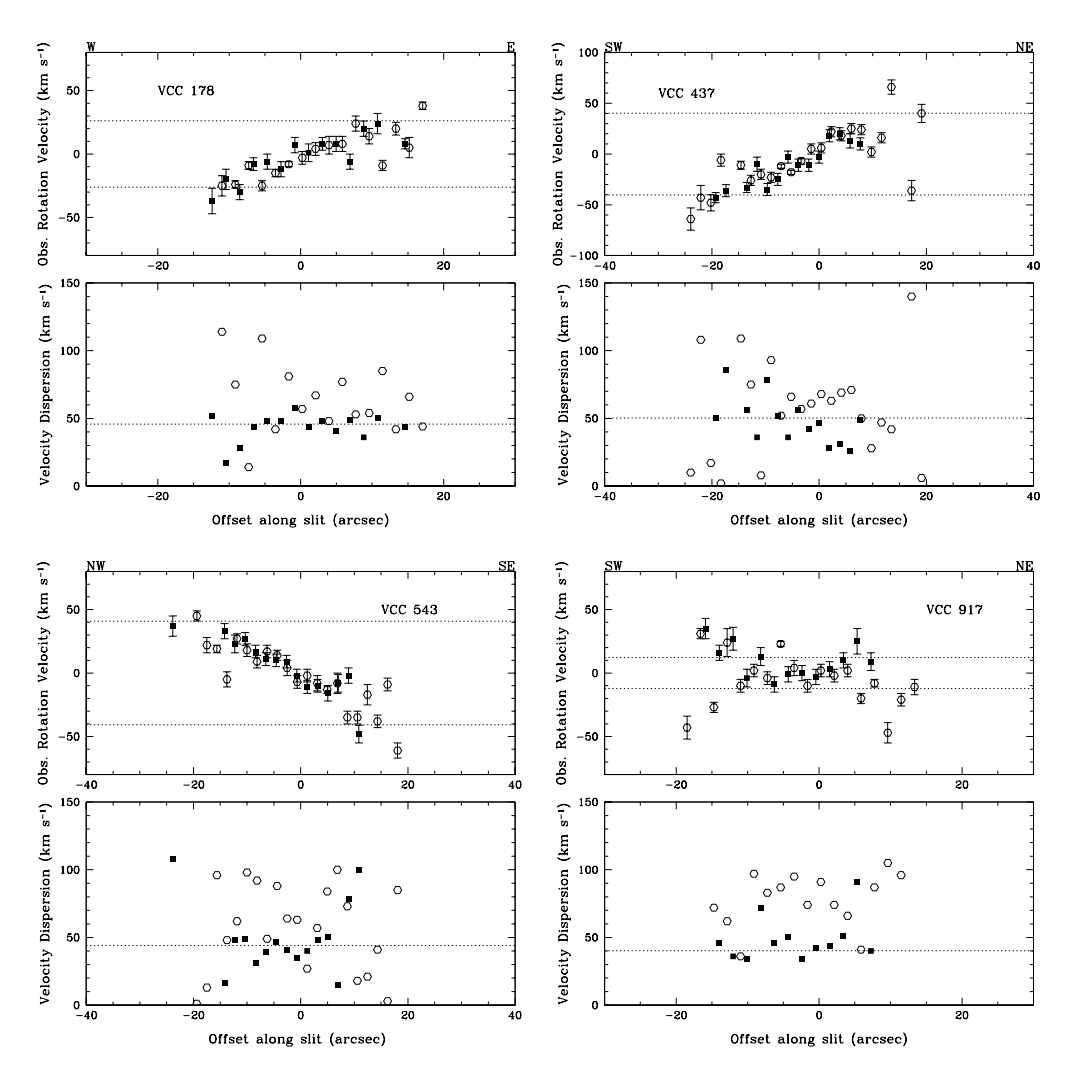
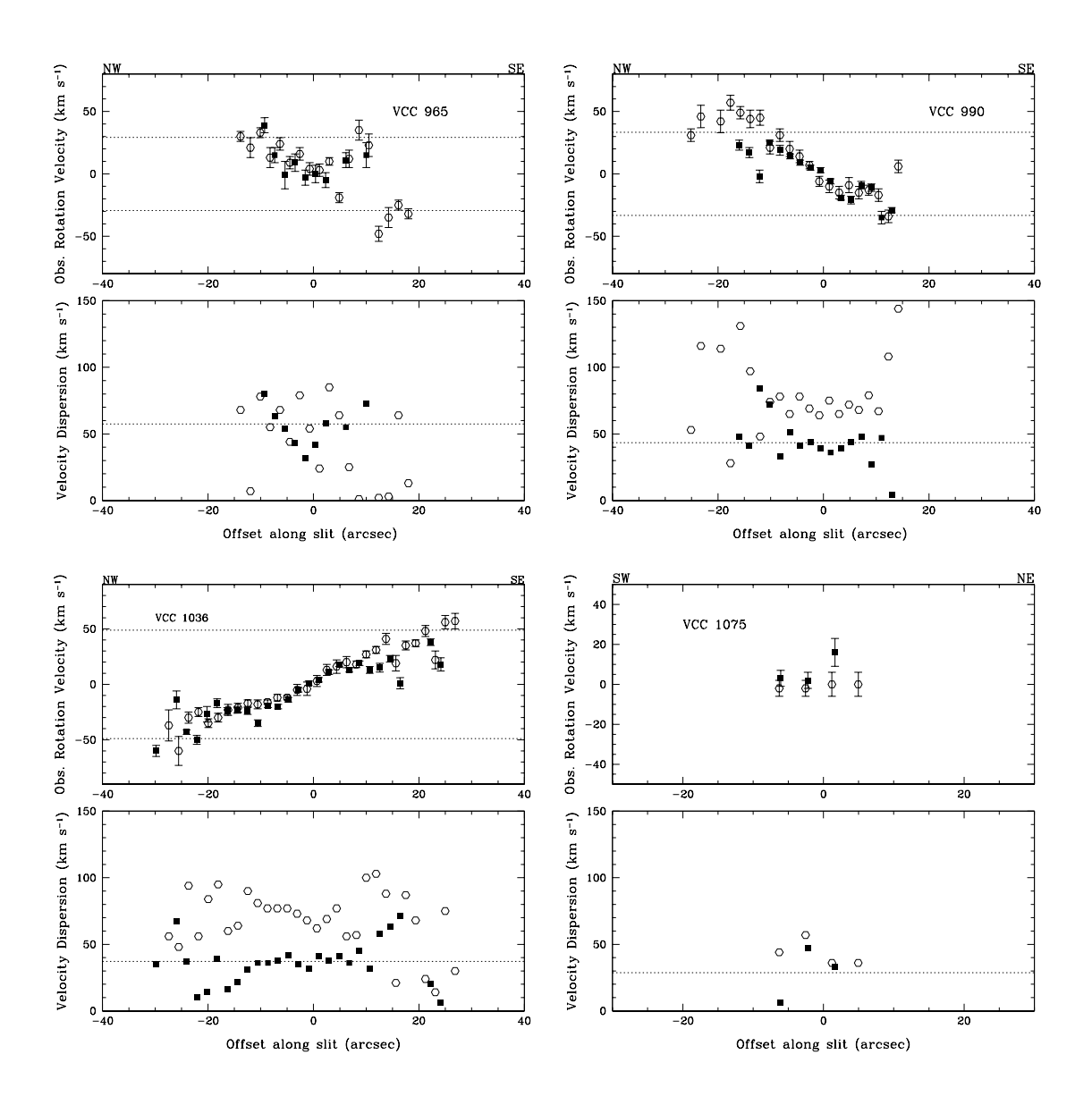
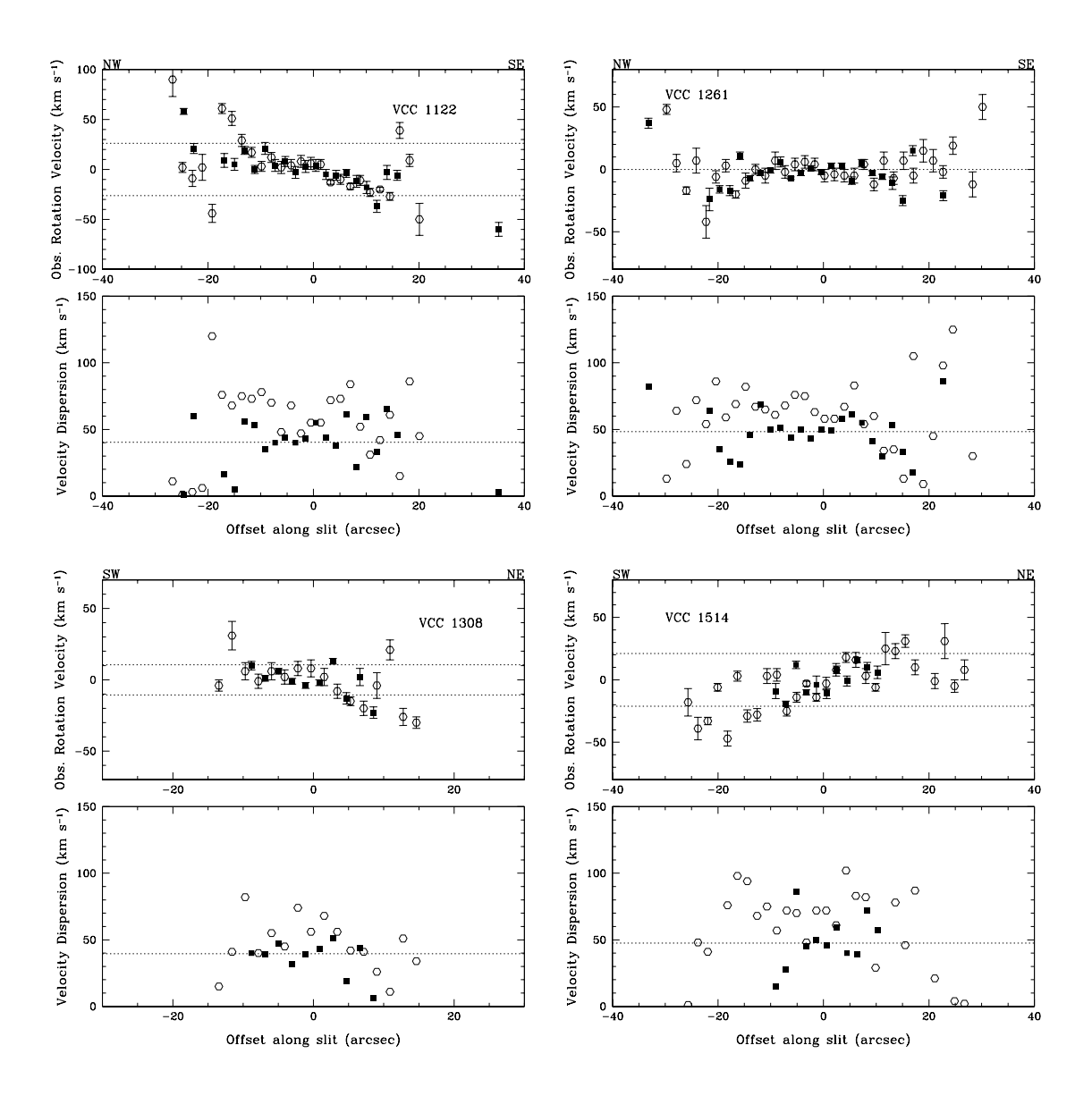
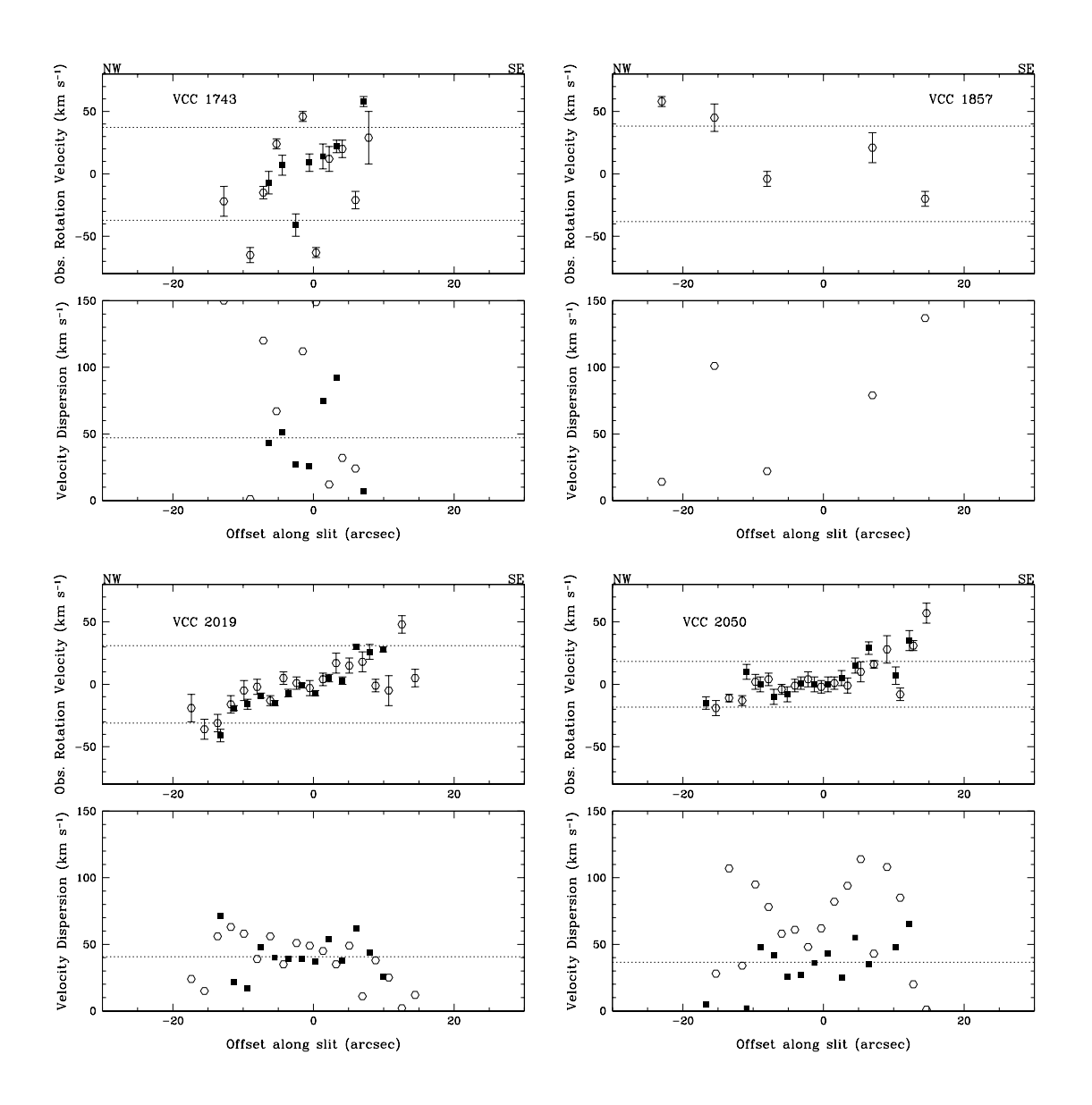


Fig. 3.— Rotation curves of sixteen dwarf elliptical galaxies. The top panel shows the rotation curve derived from the Mg Ib (open circles) and Ca triplet (filled squares) lines. The dashed lines indicate the maximum velocity width measured from the observed rotation curve. The bottom panel shows the velocity dispersion as a function of radius as derived from the Mg Ib and Ca triplet lines. In most cases, the Mg Ib measurements are upper limits to the velocity dispersion; the dashed lines denote the mean value from the Ca triplet measurements. Seven of the sixteen dwarf galaxies have a significant velocity gradient across their stellar distribution.







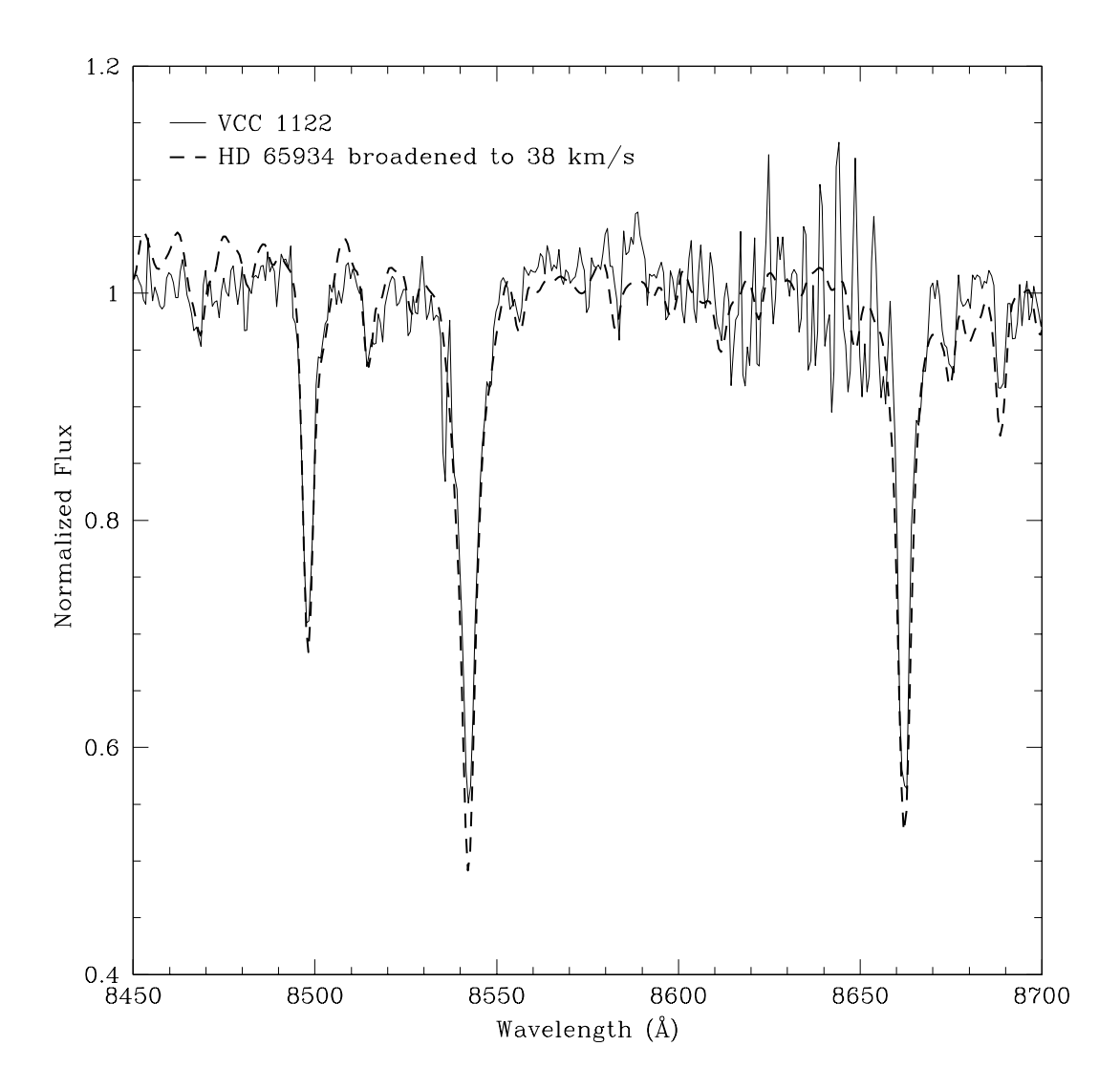


Fig. 4.— Comparison of the doppler corrected Ca triplet line profiles of the integrated spectrum of VCC 1122 and those of a G8 III template star (HD 65934) broadened with a velocity dispersion of 38 km s^{-1} . The width of the Ca lines of the template star are well matched to the galaxy spectrum, confirming that the results from the cross correlation analysis are properly calibrated.

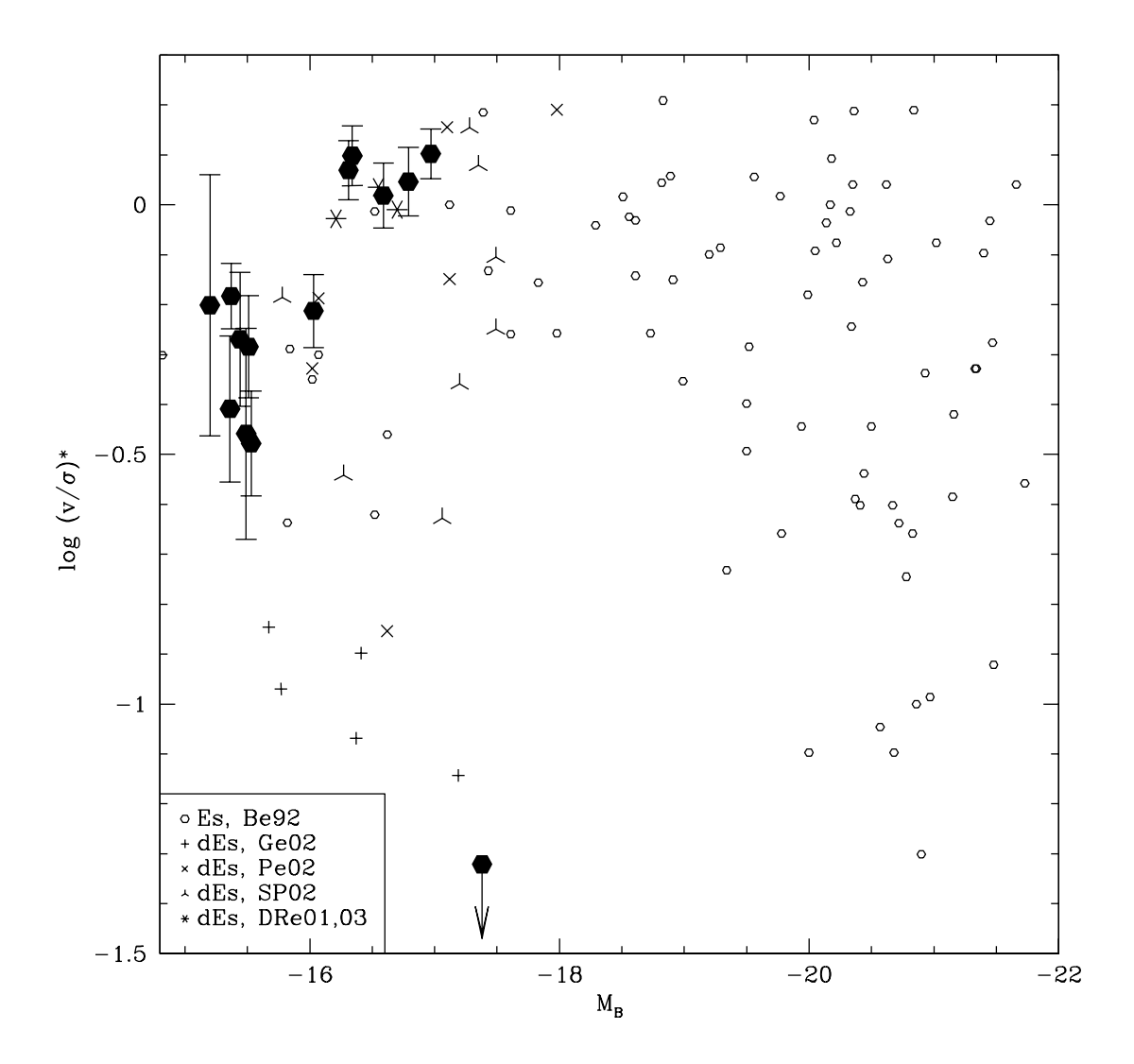


Fig. 5.— The anisotropy parameter $(v/\sigma)^*$ vs absolute magnitude for dEs and Elliptical galaxies. Filled hexagons, plus signs, crosses, triads, and stars, represent the dE galaxies from the present study, Geha et al. (2002), Pedraz et al. (2002), Simien & Prugniel (2002), and De Rijcke et al. (2001,2003) respectively. The location of VCC 1261 is shown as an upper limit since the observed velocity gradient was consistent with zero rotation. Elliptical galaxies and dEs from Bender et al. (1992) are shown with open circles. Many of the dEs in the present sample are rotationally flattened.

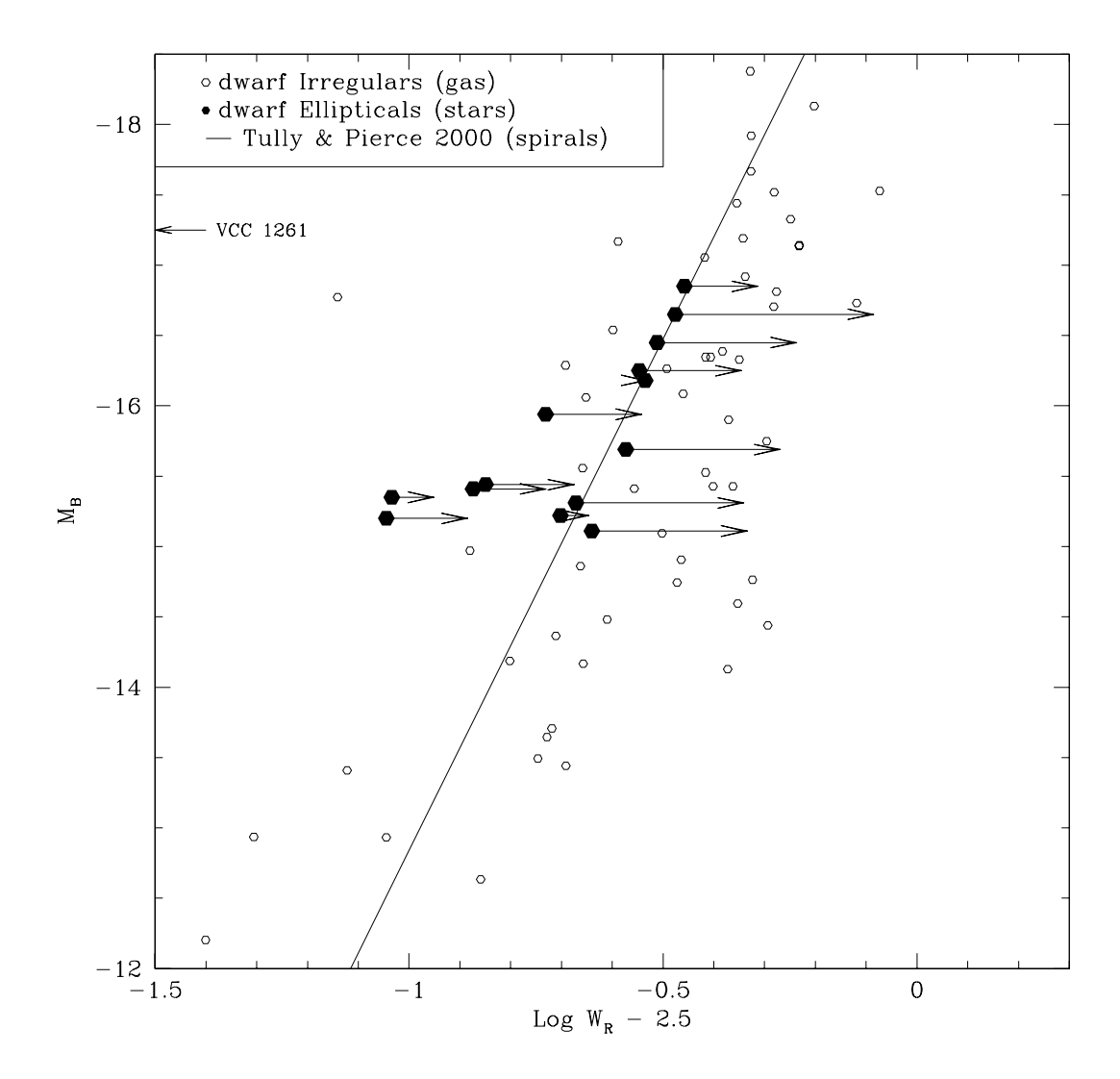


Fig. 6.— Tully Fisher relation for dIs, dEs, and spirals. The dE galaxies are shown as both filled hexagons (observed maximum rotation width) and as arrows (maximum rotation width assuming the rotation curve could be traced to 2.45 scale lengths). The open circles are the dwarf irregular galaxies compiled in van Zee (2001). The straight line shows the expected relationship for gas-rich spiral galaxies (Tully & Pierce 2000).

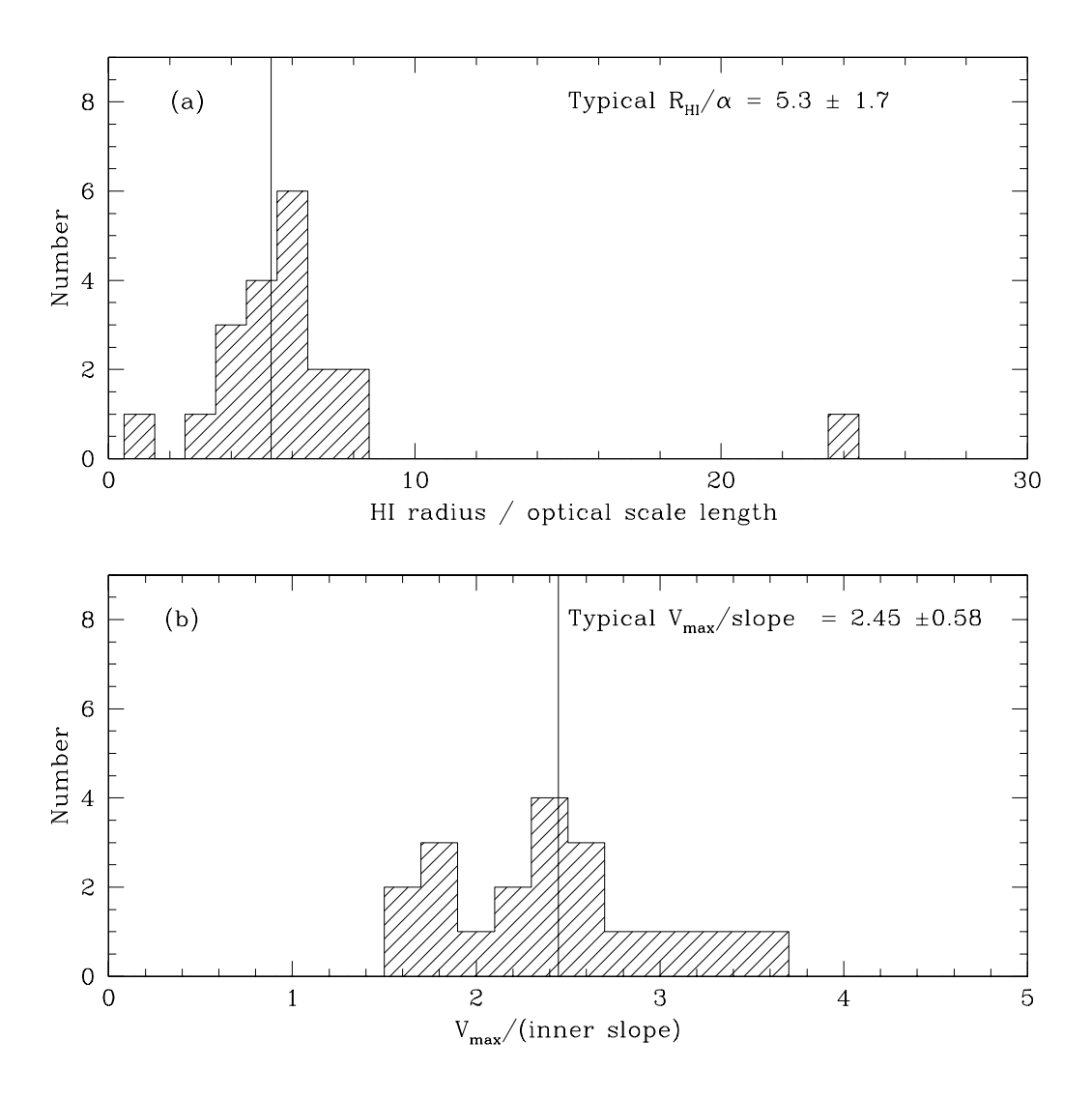


Fig. 7.— (a) Histogram of the HI-to-optical size for dwarf irregular galaxies with resolved neutral gas distributions and kinematics. The typical rotation curve for a gas-rich dwarf galaxy can be traced out to 5.3 times the optical scale length using neutral hydrogen. (b) The ratio of the maximum rotation velocity, $V_{\rm max}$, to the slope of the inner rotation curve for gas-rich dwarf irregular galaxies. The typical dwarf irregular galaxy has a $V_{\rm max}/{\rm slope}$ of 2.45 scale lengths.

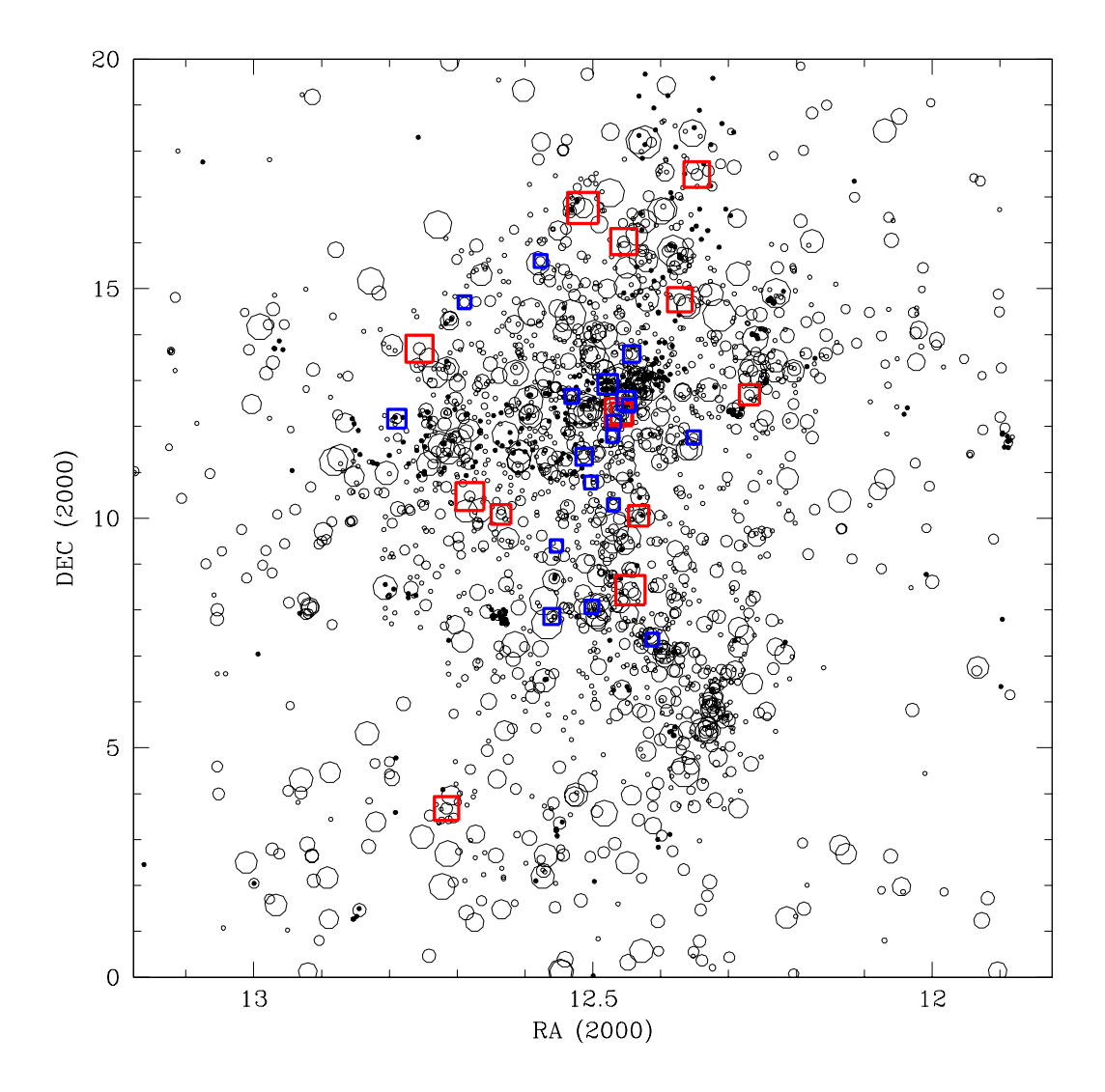


Fig. 8.— Location of the rotating (red squares) and non-rotating (blue squares) dwarf elliptical galaxies in the Virgo cluster. The relative size of the square is indicative of the galaxy's anisotropy parameter $(v/\sigma)^*$. The complete kinematic sample includes those in Geha et al. 2003; Pedraz et al. 2002; and this paper. Also shown are all cataloged galaxies believed to be in Virgo (circles). Here, the symbol size is proportional to the galaxy luminosity (open circles); galaxies in the Virgo Cluster Catalog with no listed apparent magnitudes are also included (small filled circles). There is a slight trend for the non-rotating dwarf elliptical galaxies to be located toward the cluster center or in the dense clumpy regions.